TISSUE ENGINEERING: Part C
Volume 23, Number 7, 2017

DOI: 10.1089/ten.tec.2017.0185

termis
Tissue Engineering
& Regenerative Medicine
International Society

METHODS ARTICLE

In Vivo Assessment of Engineered Skin Cell Delivery with Multimodal Optical Microscopy

Andrew J. Bower, MS,[1,2] Ziad Mahmassani, PhD,[1,3] Youbo Zhao, PhD,[1] Eric J. Chaney, BS,[1] Marina Marjanovic, PhD,[1,4] Min Kyung Lee, PhD,[5] Benedikt W. Graf, PhD,[1,2] Michael De Lisio, PhD,[3,6] Hyunjoon Kong, PhD,[5] Marni D. Boppart, ScD,[1,3] and Stephen A. Boppart, MD, PhD[1,2,4,7]

The healing process is often significantly impaired under conditions of chronic or large area wounds, which are often treated clinically using autologous split-thickness skin grafts. However, in many cases, harvesting of donor tissue presents a serious problem such as in the case of very large area burns. In response to this, engineered biomaterials have emerged that attempt to mimic the natural skin environment or deliver a suitable therapy to assist in the healing process. In this study, a custom-built multimodal optical microscope capable of noninvasive structural and functional imaging is used to investigate both the engineered tissue microenvironment and the *in vivo* wound healing process. Investigation of various engineered scaffolds show the strong relationship among the microenvironment of the scaffold, the organization of the cells within the scaffold, and the delivery pattern of these cells onto the healing wound. Through noninvasive tracking of these processes and parameters, multimodal optical microscopy provides an important tool in the assessment of engineered scaffolds both *in vitro* and *in vivo*.

Keywords: multimodal microscopy, optical imaging, *in vivo* imaging, wound healing, engineered skin

Introduction

The natural process of wound healing is significantly impaired under certain conditions such as large surface area burns and chronic wounds. Often in these cases, autografting of split-thickness skin from a donor site in the patient is the preferred treatment option and has shown good clinical outcomes. However, in patients with large area burns, it may not be possible or prudent to find a suitable donor site. In addition to this, repeated harvesting of tissue from a variety of donor sites may be necessary for large surface area and chronic wounds leading to pain, scarring, and potentially poor healing.[1] In response to this, a variety of engineered skin substitutes and cell therapies have emerged. The goal of these treatments is to mimic the natural skin environment in such a way as to promote strong healing outcomes. Currently, many split-thickness-engineered skin substitutes are available and even used clinically.[2] Most recently, autogeneic substitutes have been developed, in which cells from the patient are extracted and embedded into a support structure, which is subsequently grafted onto the skin.[3,4] However, many of these autologous therapies have been associated with unpredictable engraftment rates, further leading to poor healing outcomes.[5]

Another approach to this problem has been to develop methods to successfully deliver skin cells directly onto the wound bed without requiring the need for engraftment of an engineered tissue scaffold. These methods have shown improved wound healing, and in some cases, reduced scarring when compared with previous approaches.[6,7] Some methods for cell delivery include the development of autologous cell suspensions, which are sprayed directly onto the wound bed[8,9] as well as engineered scaffolding structures that support the flow of skin cells onto the wound bed in an organized manner.[10] However, *in vivo* assessment methods of these cell delivery approaches remain fairly primitive. In most cases, parameters such as wound size are assessed through the use of

[1]Beckman Institute for Advanced Science and Technology, University of Illinois at Urbana-Champaign, Urbana, Illinois.
[2]Department of Electrical and Computer Engineering, University of Illinois at Urbana-Champaign, Urbana, Illinois.
Departments of [3]Kinesiology and Community Health, [4]Bioengineering, and [5]Chemical and Biomolecular Engineering, University of Illinois at Urbana-Champaign, Urbana, Illinois.
[6]School of Human Kinetics, Brain and Mind Research Institute and Centre for Neuromuscular Disease, University of Ottawa, Ottawa, Canada.
[7]Department of Internal Medicine, University of Illinois at Urbana-Champaign, Urbana, Illinois.
This work was performed at the University of Illinois at Urbana-Champaign in the Beckman Institute for Advanced Science and Technology and the Institute for Genomic Biology.

photographs of the skin, and many other important outcomes such as amount and severity of scarring remain highly subjective and can vary greatly depending on the patient and physician.[11] While many *ex vivo* histological analyses can be performed to better objectively assess wound healing quality, this requires excision of skin and is generally not practical clinically. To rapidly and objectively assess the outcome of a particular therapy, it is critical to have a tool capable of noninvasively monitoring the wound bed and transplanted cells *in vivo* throughout the course of the treatment. In this study, a multimodal optical microscopy platform is utilized to track the wound healing process *in vivo* in a mouse model following treatment with a novel cell delivery therapy utilizing an engineered alginate hydrogel to deliver cells directly onto the wound bed.

Recently, intravital multimodal optical microscopy has emerged as a technique for sensitive, cellular-level resolution imaging in humans[12] as well as animal models.[13] Using a variety of optical contrast mechanisms, the native environment of tissue can be probed noninvasively, providing a wealth of information. Among the many optical imaging techniques that can be incorporated into such a multimodal optical microscope, the combination of optical coherence microscopy (OCM) and multiphoton microscopy (MPM), in particular two-photon-excited fluorescence (TPEF) microscopy and second harmonic generation (SHG) microscopy, have shown promise in the assessment of skin health and viability.[12,14,15]

OCM is a noninvasive structural optical imaging modality based on the principle of optical coherence tomography,[16] in which contrast is obtained through scattering of the incident light due to the sample structure. These scattering events occur mainly from interfaces and regions of refractive index mismatch, providing strong structural label-free contrast with high resolution.

TPEF is a fluorescence-based technique similar to fluorescence confocal microscopy that relies on the simultaneous absorption of two near-infrared photons to bring the fluorophore to an excited state.[17] Due to the optical nonlinearity of this effect, TPEF provides high axial and transverse resolution without the need for a pinhole required by fluorescence confocal microscopy. In addition to this, TPEF allows imaging deeper into scattering tissue due to the decreased scattering of the near-infrared excitation wavelengths. Together, these properties of TPEF imaging demonstrate the effectiveness of using this modality in the setting of an intravital multimodal optical microscope utilizing either endogenous fluorescence from molecules such as reduced nicotinamide adenine dinucleotide (NADH) and flavin adenine dinucleotide (FAD),[18] or from exogenous tags, dyes, or genetically expressed proteins such as green fluorescent protein (GFP).

SHG imaging is a nonlinear optical imaging technique that achieves contrast from noncentrosymmetric crystalline structures. In skin imaging, this is particularly useful as this contrast is achieved primarily from dermal collagen.[19] Thus, SHG imaging provides a tool for noninvasive imaging of the collagen support network in living skin, providing a measure of skin integrity and strength. With these techniques integrated into a single microscope platform, complementary information regarding the functional and structural parameters of the living skin environment can be obtained, providing an excellent tool for the assessment of skin health and response to a particular therapy.[20]

Previously, multimodal microscopy utilizing TPEF and SHG has been utilized for the assessment of skin under conditions of skin grafting and wounding.[14,15] In particular, these studies used a GFP-labeled bone marrow transplant (BMT) mouse model to study the BM-derived cell response to various wounding conditions. In this GFP BMT model, all BM-derived cells, including immune cells, are labeled with GFP by replacing the BM of the host animal with that of a GFP-expressing mouse. Recently, investigation of *in vitro*-engineered tissue structures have also been performed using similar multimodal optical microscopy methods.[21–23] In this study, these methods are extended to more thoroughly compare several engineered tissue scaffolds and study the effect they have on the healing process *in vivo*. The integrated OCM and MPM microscope, in conjunction with this animal model, is used to noninvasively assess both functional parameters, including the BM-derived cell response, as well as the structural integrity of the skin microenvironment *in vivo*.

Materials and Methods

Integrated multimodal optical microscope

A custom-built multimodal optical microscope capable of simultaneous OCM, TPEF, and SHG imaging was used for skin imaging (Fig. 1). This system has been described previously for *in vivo* skin imaging.[14,24] In brief, excitation light is provided by a titanium:sapphire laser (MaiTai HP; Spectra Physics). The beam is passed through 90/10 beamsplitter

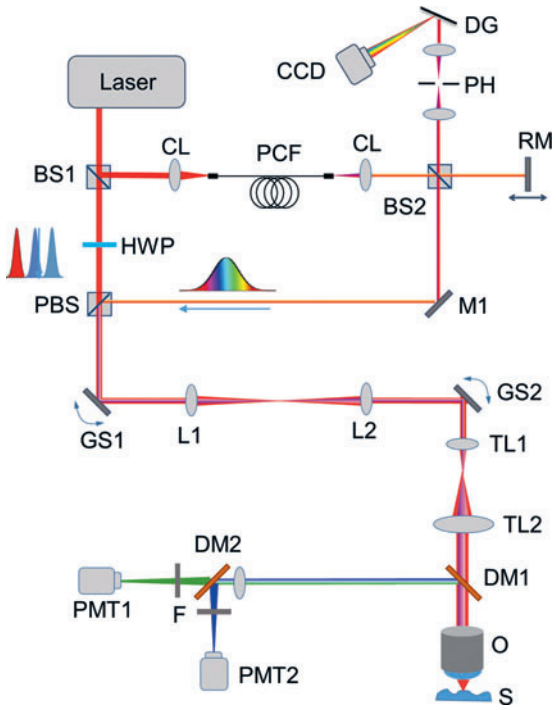

FIG. 1. Experimental setup of the integrated multimodal microscope. BS, beam splitter; CCD, charge-coupled device camera; CL, collimating lens; DG, diffraction grating; DM, dichroic mirror; GS galvo scanning mirror; HWP, half-wave plate; M, mirror; O, objective; PBS, polarizing beam splitter; PCF, photonic crystal fiber; PH, pinhole; PMT, photomultiplier tube; RM, reference mirror; TL, telescope lens. Color images available online at www.liebertpub.com/tec

separating the beams used for OCM and MPM. The OCM beam is sent through a photonic crystal fiber, which expands the bandwidth to ~100 nm full-width half-maximum. Following this, the OCM and MPM beams are recombined, sent to the sample arm of the microscope, and focused beneath the skin using a high numerical aperture (NA) objective lens (XLUMP20X, NA = 0.95; Olympus). The optical power at the focus was <10 mW. The thickness of the optical sections is ~1 μm, and the maximum imaging depth is ~150 μm. The focal spot was raster scanned transversely across the sample using a pair of computer-controlled galvanometric mirrors (MicroMax 671; Cambridge Technology). Detection of TPEF and SHG signals was performed using a pair of photomultiplier tubes (Hamamatsu H7421-40). The two channels were separated spectrally using a dichroic mirror (Semrock) and spectral filters (Semrock) chosen particularly for each modality to ensure that minimal cross talk occurred between the detection channels. The OCM signal was detected in a custom-built spectrometer. OCM images were processed online to provide structural images by performing a fast Fourier transform and identifying the corresponding *en face* frame in each dataset. To achieve a large field-of-view, sample scanning following the acquisition of each frame was performed using a three-axis computer-controlled motorized stage (Newport M-VP-25XL-XYZL). Finally, the images were stitched together into a large field-of-view mosaic. Data acquisition was performed through custom-built LabVIEW software controlling the acquisition, sample scanning, and raster scanning.

Fabrication of vertically oriented microchanneled alginate hydrogels

Fabrication of alginate hydrogels followed procedures similar to those in previous studies.[25,26] Sterile, alginate substituted with oligopeptides containing the Arg-Gly-Asp sequence was dissolved in 0.1 M 2-(*N*-morpholino)ethanesulfonic acid (MES) buffer (pH 6.5) at a concentration of 2% (w/v). The alginate solution was sequentially mixed with 1-hydroxybenzotriazole (Hobt; Fluka), 1-ethyl-3-(3-dimethylaminopropyl)carbodiimide (EDC; Sigma-Aldrich), and adipic acid dihydrazide (AAD; Sigma-Aldrich). The molar ratio of EDC:Sulfo-NHS:AAD was kept constant at 1.0:1.0:0.2. The molar ratio between AAD and uronic acid of alginate was also kept constant at 0.2:1.0. The pregelled solution was placed in a space between two glass plates separated by a 1 mm spacer. After 10 min, hydrogel disks with 5 mm-diameters were punched out and incubated in deionized water at room temperature for 12 h. Then, each gel disk was placed on top of a copper plate with thickness of 0.5 mm. The lower part of the copper plate was placed in contact with a liquid nitrogen bath for 5 min, to decrease the copper plate temperature to near −200°C. The gel disk was surrounded by polystyrene foam to create a uniaxial temperature gradient. The volumes of the hydrogel and the liquid nitrogen were kept constant between batches, to obtain reproducible results. The resulting frozen gel was lyophilized to remove ice columns and, in turn, introduce hollow microchannels with 0.1 mm diameter.

Fabrication of randomly oriented microporous alginate hydrogels

Separately, the microporous hydrogel was prepared by placing the alginate hydrogel in a copper container at −200°C. The diameter of the copper container was designed to be equivalent to a diameter of the hydrogel to make the bottom and wall of the hydrogel disk contact with the surface of the copper container. Again, the frozen hydrogel was lyophilized to remove ice from the matrix. The dehydrated sample was rehydrated with aqueous media containing cells.

GFP BM transplant mouse model

All animal procedures were performed under protocols approved by the Institutional Animal Care and Use Committee (IACUC) at the University of Illinois at Urbana-Champaign. BMTs were performed in 10–12-week-old recipient female wild-type C57BL/6 mice as previously described.[27] Male transgenic mice with global GFP expression [C57BL/6-Tg (CAG-EGFP) 10sb/J] were used as BM donors.[28] Donor mice were sacrificed by CO_2 inhalation, and BM was harvested from their hind limbs (femur and tibia). The hind limb bones were extracted, and the GFP BM was flushed using a 25-gauge needle and syringe with 1 mL of sterile phosphate-buffered saline (PBS). Cells were counted and diluted to a concentration of $\sim 7 \times 10^6$ cells/mL and kept on ice before transplantation. Following radiation treatment in recipient mice from a cobalt-60 source (two doses of 6 GY, administered 4 h apart), donor BM cells were transplanted in recipient mice via retro-orbital injection.[29]

Cell delivery procedure

Microchanneled alginate hydrogels were initially seeded with DiI-labeled C57/BL6 mouse dermal fibroblasts at a density of 1 million cells. Cells were suspended in 20 μL of culture media, and pipetted onto the dehydrated lyophilized scaffold. Upon contact with the media, the scaffolds drew in the cells and media as it rehydrated, allowing an even distribution of cells throughout the scaffold. The fibroblasts were cultured within the scaffold for 2 days. Under anesthesia, the back skin of GFP BMT mice was shaved to remove all hair from the wound site and cleaned thoroughly using isopropyl alcohol. Following this, a 5 mm diameter full-thickness skin wound was made on the GFP BMT animal that was to receive treatment.

Immediately following wounding, the alginate hydrogel was placed directly on the wound site and animals were bandaged using a transparent bandage (Nexcare Tegaderm), followed by a second more sturdy bandage (Band-Aid Tough Strips) to ensure that the scaffold would not be removed by the animal, as well as to prevent photobleaching of the DiI-labeled fibroblasts. Mice were then allowed to recover from anesthesia and were returned to their cages. Two days following wounding and grafting, bandages were removed, and the alginate hydrogel scaffold was extracted. Wounds were imaged directly following scaffold removal, and follow-up imaging was performed 10 days after wounding. Removed scaffolds were also imaged immediately following extraction to determine the presence of any remaining cells and the extent of the response from the GFP-labeled BM-derived cells.

Results

Multimodal imaging of alginate hydrogels

Multimodal imaging of the unseeded alginate hydrogels was first performed to assess the structure and viability of

these samples as cell delivery tools. Imaging was performed at two laser excitation wavelengths, 800 and 920 nm, performed in rapid succession. It was found empirically that the alginate hydrogels exhibit strong autofluorescence when excited at 800 nm. However, at this wavelength, fluorescence from the DiI-labeled cells was also present. Thus, fluorescence imaging at 800 nm provided a combination of contrast from both the structure of the alginate hydrogel as well as from the seeded cell population (Fig. 2a). OCM was also acquired at 800 nm (Fig. 2b) and yielded contrast mainly from the interfaces of the hydrogel, providing complementary structural information. At 920 nm excitation, it was found that the fluorescence signal from the alginate hydrogel was nearly absent, but the DiI signal from the labeled fibroblasts remained (Fig. 2c). By acquiring fluorescence images at excitation wavelengths of both 800 and 920 nm and coregistering the data in an appropriate color map, the fluorescence contributions of the cells and alginate hydrogel scaffold could be isolated and better visualized (Fig. 2d). This imaging strategy was utilized to further assess the effect of various structural parameters of the scaffold on the seeded cell population.

In vitro *assessment of alginate hydrogel scaffolds*

To better understand the delivery mechanism of cells within the hydrogel scaffolds, the effect of cell organization and mobility within the hydrogel scaffold microenvironment was investigated. In particular, the effect of the orientation of the micropores within the hydrogel scaffold on the profile of cellular distribution was studied. Hydrogel scaffolds are capable of being produced with transversely-, vertically-, or randomly-oriented microchannels or micropores relative to the plane of the wound bed. In scaffolds with randomly oriented micropores, each micropore was independently oriented in a random direction. As the goal is to use these scaffolds to deliver cells onto the wound bed, only vertically- (Fig. 3a, c) and randomly oriented (Fig. 3b, d) scaffolds were investigated, as the transverse microchanneled scaffolds were not likely to efficiently deliver cells onto the wound bed. Two days following the initial fibroblast seeding procedure, hydrogel scaffolds were imaged using the integrated OCM and MPM microscope. In vertically oriented scaffolds, it was observed that cells tended to form small clusters within the individual channels in the scaffold (Fig. 3c). In contrast to this, large clusters of cells with dimensions larger than the average channel size were observed in the randomly oriented scaffolds (Fig. 3d). In both cases, cells tended to be found in isolated clusters within the micropores of the scaffold. In addition to this, the cell clusters were observed to be distributed relatively homogeneously throughout both the vertically- and randomly oriented scaffolds.

In vivo *tracking of delivered cells in GFP BMT animals*

Immediately following imaging of the cell-seeded scaffolds, the scaffolds were implanted directly onto the wound

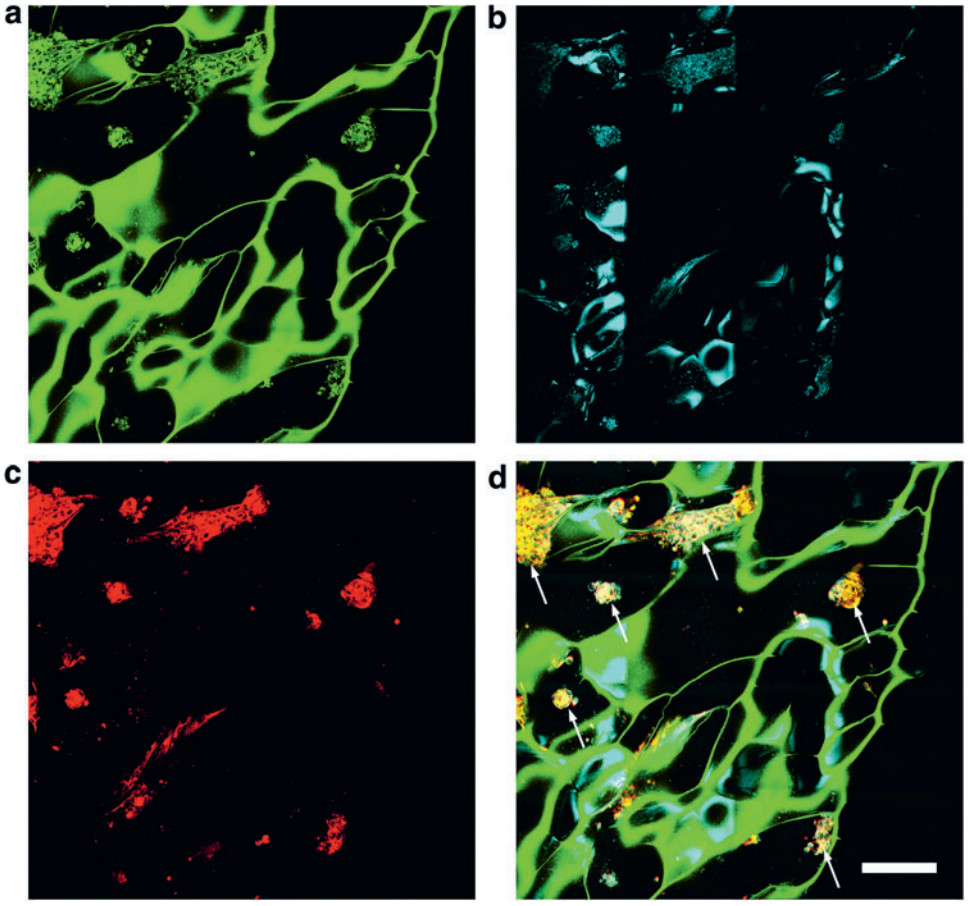

FIG. 2. Multimodal microscopy imaging of microchanneled alginate hydrogel scaffolds. **(a)** TPEF imaging at 800 nm excitation allows visualization of the scaffold and seeded fibroblasts. **(b)** OCM imaging provides structural contrast of the hydrogel scaffold. **(c)** TPEF imaging at 920 nm excitation isolates the cells from the scaffold. **(d)** The overlay of all imaging modalities provides the location of cells in the context of the microchannels within the scaffold microenvironment. *White arrows* correspond to locations of seeded cells in the microchanneled scaffolds. Color key: *Green*, TPEF at 800 nm; *Red*, TPEF at 920 nm from DiI labeled fibroblasts; *Cyan*, OCM. Scale bar is 250 μm. OCM, optical coherence microscopy; TPEF, two-photon-excited fluorescence. Color images available online at www.liebertpub.com/tec

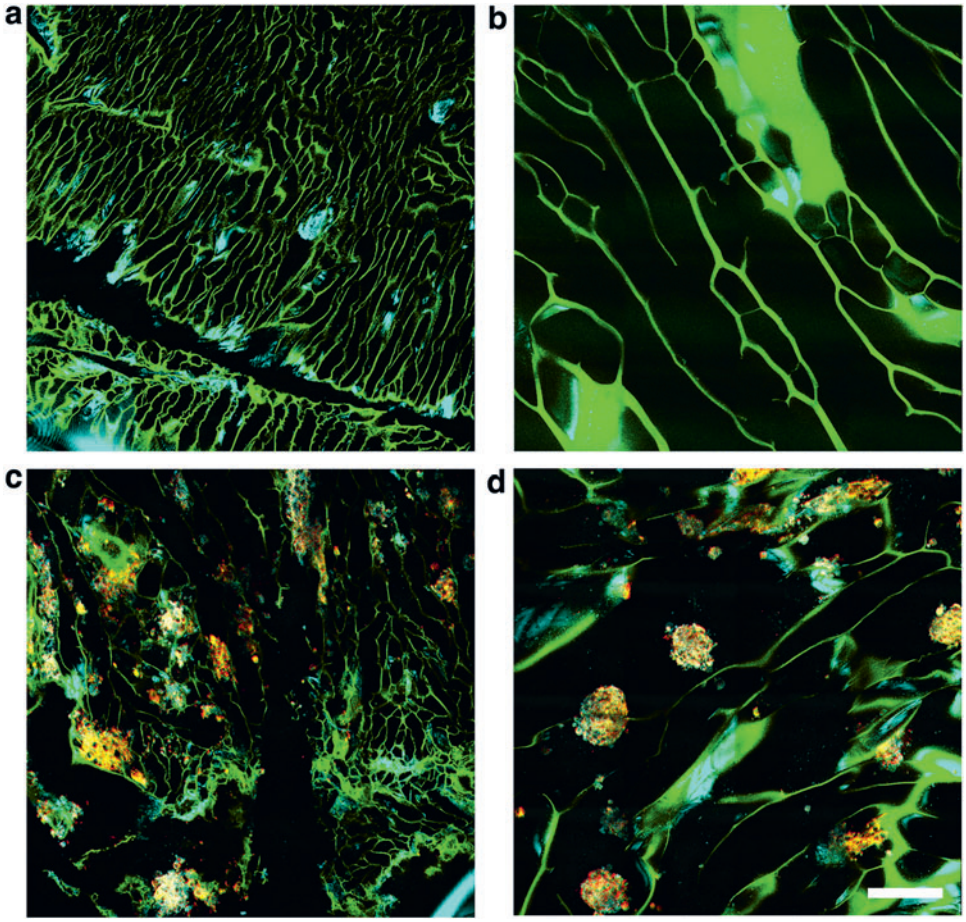

FIG. 3. Comparison of microchannel geometries in alginate hydrogel scaffolds. **(a)** Vertical microchannels without seeded fibroblasts. **(b)** Random microchannels without seeded fibroblasts. **(c)** Vertical microchannels with seeded fibroblasts. (d) Random microchannels with seeded fibroblasts. Color key follows from Figure 2. Scale bar is 250 μm. Color images available online at www.liebertpub.com/tec

bed such that the imaged side of the scaffold was in contact with the wound bed. Animals were immediately bandaged, and scaffolds remained on the wound for 2 days, after which the bandages and scaffolds were removed. Subsequently, the *in vivo* wound bed was imaged using the integrated OCM and MPM microscope. Imaging 2 days following wounding and implantation of the hydrogel scaffolds revealed the presence of DiI-labeled cells in the wound bed for scaffolds seeded with cells, compared with control animals implanted with control scaffolds that did not contain any fibroblasts (Fig. 4a).

Due to the large size of the wound and the limited extent of the practical imaging range, it was not possible to image the entire wound bed. Thus, images were acquired from approximately the center of the wound bed. In addition to this, it was observed that scaffolds with vertical microchannels tended to yield higher densities of delivered cells, based on the images acquired from the wound bed immediately following scaffold removal. After imaging, bandages (but no scaffolds) were replaced over the wound to prevent photobleaching of the delivered DiI-labeled fibroblasts. Ten days following wounding, bandages were again removed, and wounds were imaged to assess the wound microenvironment and identify the presence of any remaining fibroblasts delivered by the hydrogel scaffolds. In the wounds treated with the vertically oriented fibroblast-seeded hydrogels, the presence of DiI-labeled fibroblasts was confirmed 10 days following treatment, providing evidence of the extended contributions of this cell therapy approach. In addition to this, the GFP BM-derived cells appeared morphologically distinct, compared with the GFP BM-derived cells observed 2 days following wounding (Fig. 4b, arrows in c). On Day 2, these cells appeared more spherical or elliptical in shape, while on Day 10, cells were observed to have a more dendritic morphology. These dendritic GFP BM-derived cells also appeared to cluster around the deposited DiI-labeled fibroblasts when treated with vertically oriented hydrogels containing DiI-labeled cells (Fig. 4c, column 2), demonstrating an evident BM-derived cell response to the introduction of these foreign cells. Finally, in several cases, the presence of DiI-labeled fibroblasts was associated in several instances with the presence of SHG contrast from thick collagen patches (Fig. 4a, c—vertical with cells), suggesting the production of collagen from these newly deposited fibroblast cells.

Infiltration of BM-derived cells into hydrogel scaffolds

In addition to the multimodal imaging of the *in vivo* wounds treated with fibroblast-seeded scaffolds, the scaffolds themselves were imaged *ex vivo* immediately following removal after 2 days of direct contact with the wound bed of the GFP BMT mice (Fig. 5). Imaging of the *ex vivo* hydrogels revealed the absence of DiI-labeled fibroblasts in the scaffolds with vertically oriented microchannels (Fig. 5c). However, in scaffolds with randomly oriented micropores, some patches of

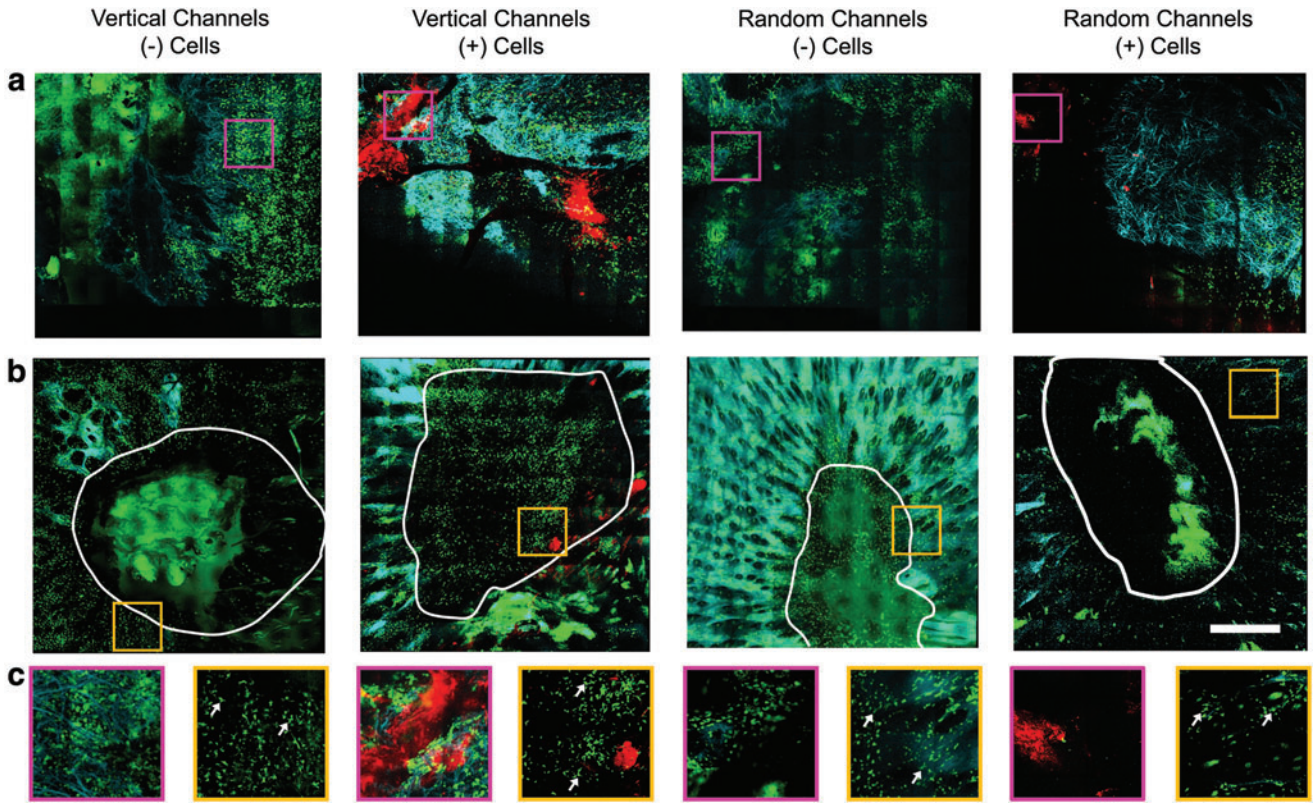

FIG. 4. *In vivo* multimodal microscopy images of wounds treated with microchanneled alginate hydrogel scaffolds at **(a)** Day 2 and **(b)** Day 10 following wounding. **(c)** Zoomed regions from the corresponding boxes in **(a)** and **(b)**. *White lines* are used to outline the wound boundary. *White arrows* correspond to GFP BM-derived cells with dendritic morphology. Color key: *Green*, GFP fluorescence; *Cyan*, SHG; *Red*, DiI fluorescence from labeled fibroblasts delivered by scaffolds. Scale bar is 500 μm. BM, bone marrow; GFP, green fluorescent protein; SHG, second harmonic generation. Color images available online at www.liebertpub.com/tec

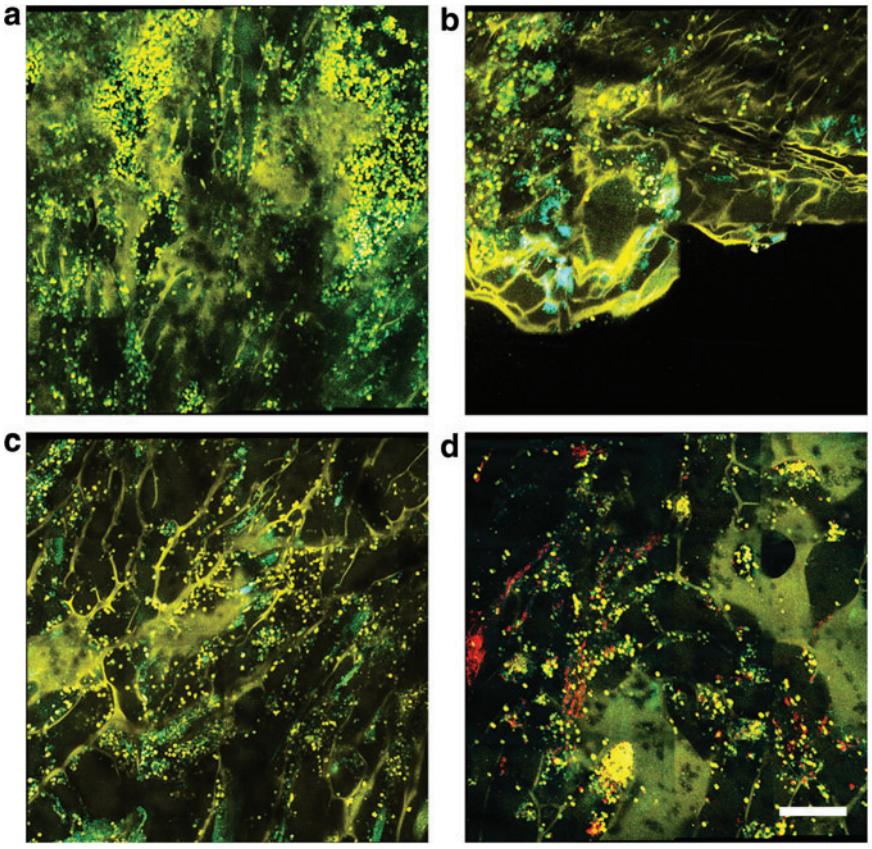

FIG. 5. Multimodal optical images of microchanneled alginate hydrogel scaffolds after removal from the wound 2 days following treatment with **(a)** vertical microchannels cultured without fibroblasts, **(b)** random microchannels without fibroblasts, **(c)** vertical microchannels with fibroblasts, and **(d)** random microchannels with fibroblasts. Color key: *Yellow*, TPEF at 800 nm; *Green*, GFP fluorescence; *Cyan*, OCM; *Red*, DiI fluorescence from labeled fibroblasts. Scale bar is 250 μm. Color images available online at www.liebertpub.com/tec

clustered DiI-labeled fibroblasts were observed (Fig. 5d). This observation implies that cells were more likely to be delivered from the scaffolds and onto the wound bed using hydrogels with vertically oriented microchannels, compared with those with randomly oriented micropores. In addition to this, a large presence of spherically shaped GFP BM-derived cells were observed to have infiltrated into the micropores of both the vertically- and randomly oriented hydrogels, indicating an evident response to the hydrogel scaffold in both conditions.

Discussion

The developed imaging protocol for the *in vitro* investigation of microporous alginate hydrogels represents a powerful tool for the analysis of these constructs before application onto wounds. Through the multimodal imaging system and the cell labeling strategy used in this study, DiI-labeled fibroblasts can be easily separated from the fluorescence of the hydrogel scaffold. It is worth noting that in the case that differently engineered scaffolds are used for similar studies, the fluorescence properties of the particular scaffold must be determined to utilize methods such as these. If the scaffold is not autofluorescent or the fluorescent signal is not separable from the cell labels being utilized, this may present challenges in identifying the spatial positions of the cells in the context of the scaffold geometry.

It is also important to note that the DiI fluorescence intensity will decrease proportionally with cell proliferation. Thus, careful attention must be paid when attempting to use similar methods for long-term time-lapse imaging of the wound healing process. OCM provides further structural information when combined with these, allowing visualization of the channel microstructures within the hydrogel. By identifying the spatial positions of the cells within the scaffold microenvironment, the direct influence of channel size and orientation on cell aggregation and organization can be determined in a straightforward manner. This provides a useful method for screening or monitoring the hydrogel scaffold before application or implantation, and may give further information about particular scaffold microstructure, orientation, cell density, and cell type, especially when correlated with healing outcomes at the conclusion of an intervention or treatment.

Multimodal optical microscopy allows for the nonintrusive study of the seeded cells in the alginate hydrogel without perturbing the natural environment. This permits both study of the cell organization and dynamics within various scaffold microenvironments as well as evaluation and monitoring of cell conditions within the scaffold before being applied to the wound. Multimodal images of the scaffolds show strong correlations between channel size, orientation, and cell aggregation or cluster density. Seeded cells within scaffolds produced with randomly oriented micropores were observed to form large clusters within the channels of the scaffold, compared with the cells in scaffolds with vertically oriented microchannels, which were observed to form smaller, less dense clusters more uniformly throughout the hydrogel scaffold. In scaffolds with randomly oriented micropores, it is likely that the large, dense clusters of cells form due to the merging of several porous channels. Due to the fact that these randomly oriented scaffolds contain a network of connected channels, it is reasonable to expect that the cells navigate these channels to form the large clusters that are observed. In contrast to this, cells within vertically oriented scaffolds are not observed to form these large clusters, as these microchannels do not form connected networks of channels.

Due to the observed clustering of the DiI-labeled cells in both vertically- and randomly-oriented hydrogels, the delivery of nonuniform clusters of cells for both orientations was observed, with more cells being delivered in the case of vertically oriented hydrogels. The ability to track large populations of BM-derived GFP cells in the hydrogel scaffold following scaffold removal provides a method for tracking the immune response to externally engineered materials, which may be useful in determining their efficacy in the treatment of wounds. From the images of the extracted hydrogels, it was also discovered that the presence of the scaffold invoked an evident BM-derived cell response, as seen by the presence of large populations of GFP BM-derived cells. The fact that some DiI-labeled cells remained in the scaffolds with randomly oriented micropores also provides evidence that the scaffold microenvironment plays an important role in the efficacy of these cell therapies.

Tracking of these parameters using this multimodal microscope provides a set of methods that can be used to analyze potential cell delivery therapies in terms of their ability to transport cells onto the wound bed. In the future, combining these methods with quantitative imaging methods to determine important metrics such as the number and spatial distribution patterns of the delivered cells could further enhance the power of these methods in the *in vivo* and *in vitro* assessment of engineered tissue constructs. In addition to this, histological methods can also be used as a gold standard to determine treatment efficacy and confirm observations from the *in vivo* microscopy data.

These two cell delivery strategies were directly observed after examination of wounds *in vivo* utilizing the same integrated multimodal optical microscope. In addition to this, the use of the GFP BMT animal model allowed visualization of the interactions between the delivered fibroblasts and the native BM-derived cells of the mouse, which provided functional information regarding the native BM-derived cell response to the treatment. The ability to also detect collagen from the SHG signals in the wound bed led to the observations of the colocalization of the delivered fibroblasts in the vicinity of dense patches of collagen. As fibroblasts are known for their ability to produce collagen, especially in the presence of wound healing,[30] this suggests that these delivered fibroblasts were either producing collagen or positioned themselves near existing collagen fibers to further assist the wound healing process. The ability to simultaneously determine interactions such as this in the complex *in vivo* wound healing environment demonstrates the power of this multimodal imaging approach.

Conclusions

In this study, a custom-built multimodal optical microscope was used to investigate the use of alginate hydrogel scaffolds as cell delivery vehicles for the treatment of large wounds in GFP BMT mice. This integrated multimodal imaging platform based on different, yet, complementary contrast mechanisms provides an important method for

investigating novel treatments for cell delivery. In particular, the microscope was able to noninvasively probe both the hydrogel scaffold and the *in vivo* wound microenvironments, allowing observations of the delivered cell dynamics as well as the interactions among the host immune system, collagen structure, and delivered cells. In this way, multimodal optical microscopy represents a powerful tool for assessing wound healing therapies based on novel engineered biomaterials.

Acknowledgments

We thank Darold Spillman for assistance with logistical and information technology support. This research was supported, in part, by grants from the National Science Foundation (STC-EBICS Grant CBET-0939511 to H.K. and CBET 10-33906) and the National Institutes of Health (NIH R01 EB023232). A.J.B. was supported, in part, by a National Science Foundation Graduate Research Fellowship (DGE-1144245) and by a UIUC ECE Distinguished Research Fellowship. Additional information can be found at http://biophotonics.illinois.edu.

Disclosure Statement

No competing financial interests exist.

References

1. Supp, D.M., and Boyce, S.T. Engineered skin substitutes: practices and potentials. Clin Dermatol **23,** 403, 2005.
2. Falabella, A.F., Valencia, I.C., Eaglstein, W.H., and Schachner, L.A. Tissue-engineered skin (Apligraf) in the healing of patients with epidermolysis bullosa wounds. Arch Dermatol **136,** 1225, 2000.
3. Boyce, S.T., Goretsky, M.J., Greenhalgh, D.G., Kagan, R.J., Rieman, M.T., and Warden, G.D. Comparative assessment of cultured skin substitutes and native skin autograft for treatment of full-thickness burns. Ann Surg **222,** 743, 1995.
4. Limat, A., Mauri, D., and Hunziker, T. Successful treatment of chronic leg ulcers with epidermal equivalents generated from cultured autologous outer root sheath cells. J Invest Dermatol **107,** 128, 1996.
5. Halim, A.S., Khoo, T.L., and Shah, J.M.Y. Biologic and synthetic skin substitutes: an overview. Indian J Plast Surg **43,** 23, 2010.
6. Hartmann, B., Ekkernkamp, A., Johnen, C., Gerlach, J.C., Belfekroun, C., and Küntscher, M.V. Sprayed cultured epithelial autografts for deep dermal burns of the face and neck. Ann Plast Surg **58,** 70, 2007.
7. Li, J., Pincu, Y., Marjanovic, M., Bower, A.J., Chaney, E.J., Jensen, T., Boppart, M.D., and Boppart, S.A. *In vivo* evaluation of adipose- and muscle-derived stem cells as a treatment for nonhealing diabetic wounds using multimodal microscopy. J Biomed Opt **21,** 086006, 2016.
8. Falanga, V., Iwamoto, S., Chartier, M., Yufit, T., Butmarc, J., Kouttab, N., Shrayer, D., and Carson, P. Autologous bone marrow-derived cultured mesenchymal stem cells delivered in a fibrin spray accelerate healing in murine and human cutaneous wounds. Tissue Eng **13,** 1299, 2007.
9. Hanson, S.E., Bentz, M.L., and Hematti, P. Mesenchymal stem cell therapy for nonhealing cutaneous wounds. Plast Reconstr Surg **125,** 510, 2010.
10. El-Sherbiny, I.M., and Yacoub, M.H. Hydrogel scaffolds for tissue engineering: progress and challenges. Glob Cardiol Sci Pract **2013,** 38, 2013.
11. Idriss, N., and Maibach, H.I. Scar assessment scales: a dermatologic overview. Skin Res Technol **15,** 1, 2009.
12. Graf, B.W., and Boppart, S.A. Multimodal *in vivo* skin imaging with integrated optical coherence and multiphoton microscopy. IEEE J Sel Top Quantum Electron **18,** 1280, 2012.
13. Koenig, K. Hybrid multiphoton multimodal tomography of *in vivo* human skin. Intravital **1,** 11, 2012.
14. Graf, B.W., Bower, A.J., Chaney, E.J., Marjanovic, M., Adie, S.G., De Lisio, M., Valero, M.C., Boppart, M.D., and Boppart, S.A. *In vivo* multimodal microscopy for detecting bone-marrow-derived cell contribution to skin regeneration. J Biophotonics **7,** 96, 2014.
15. Graf, B.W., Chaney, E.J., Marjanovic, M., Adie, S.G., De Lisio, M., Valero, M.C., Boppart, M.D., and Boppart, S.A. Long-term time-lapse multimodal intravital imaging of regeneration and bone-marrow-derived cell dynamics in skin. Technology **1,** 8, 2013.
16. Izatt, J.A., Swanson, E.A., Fujimoto, J.G., Hee, M.R., and Owen, G.M. Optical coherence microscopy in scattering media. Opt Lett **19,** 590, 1994.
17. Denk, W., Strickler, J., and Webb, W. Two-photon laser scanning fluorescence microscopy. Science **248,** 73, 1990.
18. Skala, M.C., Riching, K.M., Gendron-Fitzpatrick, A., Eickhoff, J., Eliceiri, K.W., White, J.G., and Ramanujam, N. *In vivo* multiphoton microscopy of NADH and FAD redox states, fluorescence lifetimes, and cellular morphology in precancerous epithelia. Proc Natl Acad Sci U S A **104,** 19494, 2007.
19. Campagnola, P.J., Millard, A.C., Terasaki, M., Hoppe, P.E., Malone, C.J., and Mohler, W.A. Three-dimensional high-resolution second-harmonic generation imaging of endogenous structural proteins in biological tissues. Biophys J **82,** 493, 2002.
20. Bower, A.J., Arp, Z., Zhao, Y., Li, J., Chaney, E.J., Marjanovic, M., Hughes-Earle, A., and Boppart, S.A. Longitudinal *in vivo* tracking of adverse effects following topical steroid treatment. Exp Dermatol **25,** 362, 2016.
21. Zhao, Y., Graf, B.W., Chaney, E.J., Mahmassani, Z., Antoniadou, E., DeVolder, R., Kong, H., Boppart, M.D., and Boppart, S.A. Integrated multimodal optical microscopy for structural and functional imaging of engineered and natural skin. J Biophotonics **5,** 437, 2012.
22. Liang, X., Graf, B.W., and Boppart, S.A. Imaging engineered tissues using structural and functional optical coherence tomography. J Biophotonics **2,** 643, 2009.
23. Tan, W., Sendemir-Urkmez, A., Fahrner, L.J., Jamison, R., Leckband, D., and Boppart, S.A. Structural and functional optical imaging of three-dimensional engineered tissue development. Tissue Eng **10,** 1747, 2004.
24. Vinegoni, C., Ralston, T., Tan, W., Luo, W., Marks, D.L., and Boppart, S.A. Integrated structural and functional optical imaging combining spectral-domain optical coherence and multiphoton microscopy. Appl Phys Lett **88,** 053901, 2006.
25. Lee, M.K., Rich, M.H., Shkumatov, A., Jeong, J.H., Boppart, M.D., Bashir, R., Gillette, M.U., Lee, J., and Kong, H. Glacier morraine formation-mimicking colloidal particle assembly in microchanneled, bioactive hydrogel for guided vascular network construction. Adv Healthc Mater **4,** 2, 2015.

26. Lee, M.K., Rich, M.H., Lee, J., and Kong, H. A bio-inspired, microchanneled hydrogel with controlled spacing of cell adhesion ligands regulates 3D spatial organization of cells and tissue. Biomaterials **58,** 26, 2015.
27. De Lisio, M., and Parise G. Characterization of the effects of exercise training on hematopoietic stem cell quantity and function. J Appl Physiol **113,** 1576, 2012.
28. Okabe, M., Ikawa, M., Kominami, K., Nakanishi, T., and Nishimune, Y. 'Green mice' as a source of ubiquitous green cells. FEBS Lett **407,** 313, 1997.
29. Yardeni, T., Eckhaus, M., Morris, H.D., Huizing, M., and Hoogstraten-Miller, S. Retro-orbital injections in mice. Lab Anim (NY) **40,** 155, 2011.
30. Ortiz-Urda, S., Lin, Q., Green, C.L., Keene, D.R., Marinkovich, M.P., and Khavari, P.A. Injection of genetically engineered fibroblasts corrects regenerated human epidermolysis bullosa skin tissue. J Clin Invest **111,** 251, 2003.

Address correspondence to:
Stephen A. Boppart, MD, PhD
Beckman Institute for Advanced Science and Technology
University of Illinois at Urbana-Champaign
Urbana, IL 61801

E-mail: boppart@illinois.edu

Received: April 12, 2017
Accepted: May 22, 2017
Online Publication Date: July 13, 2017